Artificial Neural Networks Approach for Reduced RMS Currents in Triple Active Bridge Converters

Ahmed A. Ibrahim, Andrea Zilio, Tarek Younis, Davide Biadene, Tommaso Caldognetto, Paolo Mattavelli
Dept. of Management and Engineering (DTG)
University of Padova, Vicenza, Italy
name.surname@unipd.it

***Abstract*—Isolated multi-port converters show the merits of hosting several sources and loads with different voltage and power ratings, allowing power routing among multiple ports with high power density. However, many degrees of freedom are available for modulation, and exploiting them for optimal converter operation is challenging. This paper proposes an artificial neural network (ANN) approach that minimizes the rms ports currents of a triple active bridge (TAB) converter for the entire range of operation. The ANN is trained to determine the optimum duty-cycles for total true rms current minimization. The effectiveness of the ANN implementation is shown by considering an experimental TAB converter prototype rated $5\,\mathrm{kW}$.**

***Index Terms*—Artificial neural network (ANN), multi-port converter, triple active bridge (TAB).**

I. Introduction

Isolated multi-port converters (IMPCs) present advantageous features for accommodating loads or energy resources operating at different voltage and power levels while providing galvanic isolation between the ports and high power density [1], [2]. For these merits, applications of IMPCs can be found, for example, in electrified vehicles [3], electrified aircrafts [4], [5], and in nanogrids [6] and microgrids [7], [8]. A common IMPC topology is the triple active bridge (TAB) converter, shown in Fig. 1(a) and introduced in [9], [10]. The TAB mainly consists of three full bridges connected through a three-winding high-frequency transformer.

To control the power flow among the ports, phase shift modulation (PSM), shown in Fig. 1(b), is commonly applied, like for the case of dual active bridge (DAB) converters [11]. With PSM, the three bridges generate ac voltages v_1, v_2, v_3 with duty-cycle fixed at 50% and variable phase shifts ϕ_2 and ϕ_3. By controlling the phase-shifts magnitude and sign, it is possible to regulate the power flow intensity and direction, respectively [9]. PSM shows the advantage of simplicity, besides low switching and conduction losses at moderate to high load conditions, while operating with dc voltages such that $V_1 : V_2 : V_3 = n_1 : n_2 : n_3$. Meanwhile, switching and conduction losses increase dramatically at light-load conditions or with significant voltage mismatches among the transformer terminals.

Penta phase-shift modulation schemes, shown in Fig. 1(c), have been introduced to overcome these drawbacks [12]. By these approaches, the modulation exploits not only the phase shifts ϕ_2 and ϕ_3 but also the duty-cycles D_1, D_2, D_3. The increased number of modulation variables significantly increases

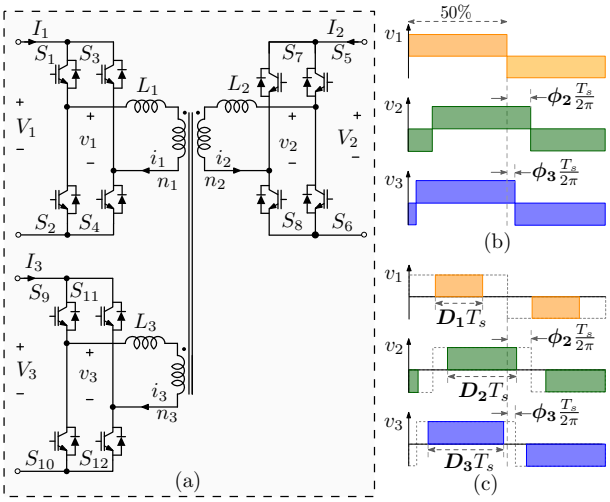

Fig. 1: (a) Triple active bridge converter; (b) phase-shift modulation; (c) penta phase-shift modulation. Modulation variable $\phi_2, \phi_3, D_1, D_2, D_3$ highlighted.

the complexity; controlling five modulation parameters gives a total number of possible switching patterns in the order of hundreds. Tackling and analyzing each switching pattern separately to find the optimum operation, for example, in terms of losses, is time-consuming or even not possible. The literature reports different approaches pursuing efficiency optimization of the converter utilizing penta phase-shift modulation [12]–[19]. Based on the current literature, the most critical limits that can be identified are the heavy mathematical analysis tools and results needed for the modeling of the TAB behavior, the inevitable mismatch among the obtained models and the actual converter operation that impairs the results of off-line search based on converters models, the use of large and complex look-up tables, and the potentially long time, local-minima issues, and inefficient transients related to on-line optimization methods.

Potential improvements are aimed herein by the application of artificial intelligence approaches. Considering the related literature, in [20] an artificial neural network (ANN) model has been built for an interleaved boost with coupled inductors (IBCI) converter, showing its merits over a look-up table from the point of view of memory usage. Such an advantage is expected to be even more appreciable with the additional degrees of freedom of a TAB. In [21] an ANN is used to

minimize the current stress for a DAB. The ANN is trained using data collected from a PLECS simulation. No additional applications of ANN for TAB modulation were found.

In this paper, an ANN approach is proposed for modeling the best modulation parameters D_1, D_2, and D_3 for a TAB converter given the operating conditions in terms of operating voltages and power flows. Optimality is measured in terms of total rms current measured at transformer ports. The ANN is trained off-line by exploiting the results from a systematic search of the optimal modulation parameters. This search is performed considering a simulation model that has been calibrated to match the operation of the real experimental TAB prototype.

The proposed approach details, implementation, and experimental verification are discussed in the following.

II. Proposed Approach

The proposed approach consists in training an ANN to find the minimum total true rms current defined as:

$$i^{rms} = \sqrt{\sum_{p=1}^{3} r_p \left(i_p^{rms}\right)^2} = f(\phi_2, \phi_3, D_1, D_2, D_3) \qquad (1)$$

where weights r_p, $p = 1, \ldots, 3$, are the equivalent path resistances of the respective p-th port. Notably, the total true rms current depends on five modulation parameters, as mentioned in Sec. I.

Solving this complex non-convex function to find the minimum total rms current is a challenging task. Herein, this complexity is overcome by a data-driven approach, exploiting the information collected from a simulation model to compute the optimal TAB modulation parameters for rms current reduction.

The training process of the ANN is done in four steps, discussed in the following sections:

1) simulation model validation and data-set collection, as described in Sec. III;
2) definition of the best ANN structure, as described in Sec. IV;
3) training of the ANN based on the collected data, as described in Sec. V;
4) validating the obtained results on the experimental prototype, as described in Sec. VI.

III. Data Collection for ANN Training

PLECS simulations have been used to generate the data-set used to train the ANN, as done in [21].

First, the simulation model has been calibrated and validated to match the experimental prototype, considering the actual transformer leakage inductance, the switching frequency, the deadtime, etc. The matching process includes matching transformer rms current and current and voltage waveforms at various test points. The rms current deviation between the two models is below 10%.

Second, a systematic, brute-force search is run on the duty-cycles D_1, D_2, D_3, testing about 512 possible combinations of duty-cycles for each power and voltage set-point. While phase-shifts ϕ_2 and ϕ_3 are adjusted by employing two separate linear regulators. The search finds duties with minimum total true rms current, and it is repeated for about $15,000$ set-points of different ports voltages and powers. The collected data-set represents the brute-force search findings, with about $15,000$ points, which is then used to train the ANN, as described in the next.

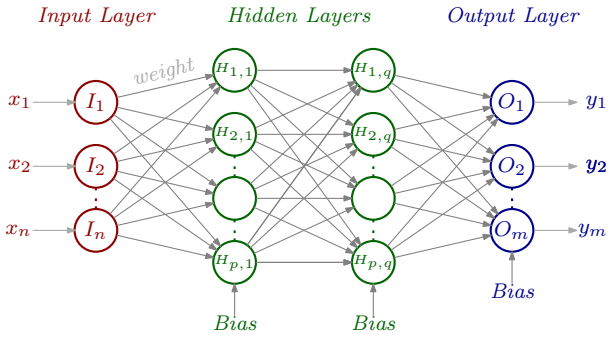

Fig. 2: Example of MLP-NN with n inputs, q hidden layers p neurons each and m outputs.

IV. ANN Basics and Chosen Structure

Among various kinds of ANNs used in the field of power electronics [22], *Multilayer Perceptron Neural Networks* (MLP-NNs) are considered in this work. In this type of network, the neurons are divided into layers that are typically fully connected. They are also called feed-forward ANNs due to the fact that the information only travels forward in the network. When the relationship between inputs and outputs is a non-linear static function, MLP-NN is the most suitable architecture of ANN to be used [23], with an appropriate number of hidden layers and neurons.

The basic elements in a MLP-NN are [24] *i*) number of layers, *ii*) number of neurons in each layer, *iii*) activation function of each layer, *iv*) algorithm used during training process.

In MLP-NNs there are at least three layers: the input, the output and the shallow layer. The internal layers between input and output are denoted as hidden layers. Commonly, the higher the problem's complexity (i.e., the complexity of the function to be estimated) the higher the number of neurons and hidden layers required. Unfortunately, it is not possible to theoretically determine *a-priori* how many hidden layers or neurons are needed for a given problem. To address this issue, a systematic analysis is carried out herein for establishing the most suitable ANN architecture.

Fig. 2 depicts a common configuration of MLP-NN, with n inputs, q hidden layers with p neurons each, and m outputs. The output of a neuron is defined as a linear combination of the inputs and the resulting output is passed to a non-linear function called activation function. The ability of an ANN to be used for the analysis of non-linear problems is given by the use of activation functions that are not linear. Among different types of activation functions [25], in this work the

sigmoid activation function is used for the deep layers while the *ReLU* one for the output layer.

A. Development of ANN

The development of an ANN aims to finding the hyperparameters. In machine learning, the hyperparameters are the variables that determine the network structure (e.g., number of layers and hidden units, activation function) and its training procedure (e.g., learning rate). Hyperparameters are set before training and if the performance, in terms of estimation error, is insufficient they need to be adapted.

The development of an ANN is divided into three steps:

1) *Preliminary operations*: given the data-set, it is split in training ($\simeq 70\,\%$), validation ($\simeq 15\,\%$) and test ($\simeq 15\,\%$). Training data are used during the learning phase, validation data are crucial to test the generalization capability of the network during training process, and the test data are used in the performance evaluation step. To make the learning process more efficient, the data-set is commonly normalized; in our case between 0 and 1.
2) *Training*: it is the most time-consuming process. The backpropagation algorithm, to update network weights and biases, is applied *n*-times, where *n* is the number of epochs. The training ends when the loss function, in this work the mean squared error (MSE), reaches a minimum or when it is constant over a certain number of epochs. The validation data-set is used to detect over/under-fitting.
3) *Performance evaluation*: the test-set is evaluated, and the obtained output is compared with the data-set output. If the performances of the ANN, in terms of error, are not sufficient, the ANN hyperparameters should be updated.

V. Development of ANN for power efficiency optimization

Several deep learning frameworks and libraries are available nowadays. Commonly used ones are, for example, Matlab Deep Learning, TensorFlow, and PyTorch. Herein, the ANN is developed on Keras TensorFlow 2.6 with Intel i9-12900KF CPU at $3.19\,\mathrm{GHz}$ and $32\,\mathrm{GB}$ memory. With this setup, the average training time is less then $20\,\mathrm{s}$.

The ANN has four inputs V_2, V_3, P_2, and P_3 and three outputs D_1, D_2 and D_3.

Being not possible, as mentioned above, to determine *a-priori* how many hidden layers or neurons are needed in each layer, a systematic, brute-force approach is adopted. As a design choice, a maximum number of layers $q_{max} = 3$, a minimum and maximum number of neurons per layer $p_{min} = 5$ and $p_{max} = 35$, respectively, were chosen.

The common hyperparameters used during the training process are reported in Tab. I.

To choose the most suitable architecture, the metrics mean absolute percentage error (MAPE), root mean square error (RMSE), and mean absolute error (MAE) are considered:

$$MAPE_i(\%) = \frac{100}{K}\sum_{k=1}^{K}\frac{|D_{k,i} - \hat{D}_{k,i}|}{D_{k,i}}, \tag{2}$$

TABLE I: Common hyperparameters used during the training process.

Parameter	Value
Optimizer	Adam
Learning Rate	0.01
Loss Function	MSE
Epochs	2000
Batch Size	256
Activation Function	Sigmoid and ReLU

TABLE II: Best architecture results

Metric	Value	HL_1	HL_2	HL_3
$RMSE$	0.017	34	33	32
$MAPE$	2.61	34	33	32
MAE	0.010	34	32	23

$$RMSE_i = \sqrt{\frac{1}{K}\sum_{k=1}^{K}\left(D_{k,i} - \hat{D}_{k,i}\right)^2}, \tag{3}$$

$$MAE_i = \frac{1}{K}\sum_{k=1}^{K}|D_{k,i} - \hat{D}_{k,i}|, \tag{4}$$

where $D_{k,i}$ is the estimated i-th duty-cycle, $\hat{D}_{k,i}$ is the i-th true duty-cycle, with $i \in \{1, 2, 3\}$, and K is the number of samples.

An algorithm is used to find the most suitable architecture. The number of neurons is varied between 5 and 35 for each layer, but configurations with one or two hidden layers are also considered. Since the initial weights of the network are chosen randomly, the entire training process (i.e., data splitting, training and compute errors) is repeated three times in order to avoid convergence at local minimum points. The results of each run, for the same configuration, are stored inside a vector and only the average is returned.

The best results in terms of RMSE, MAPE and MAE are shown in Tab. II. They were calculated using the test data-set. Fig. 3 displays the obtained performance in terms of MAPE, similar results are were achieved considering the other metrics. Considering the relative flatness of the metrics for the considered problem, the choice of the ANN architecture is done based on a trade-off between its performance in terms of errors and its complexity. The chosen ANN has 3 hidden layers with 20, 20, and 15 neurons, respectively. It allows to obtain a MAPE, on test data-set, of $2.85\,\%$, a RMSE of 0.019 and a MAE of 0.011 with a training time of around $15\,\mathrm{s}$.

Two operating points are used to visualize the performances of ANN. The voltages V_2 and V_3 are kept constant in both the cases shown in Fig. 4, while in the first case the P_3 is fixed at $500\,\mathrm{W}$ and in the second one P_2 at the same rating. In Fig. 4, the dotted lines are the data obtained from brute-force analysis and used during the training process while, the continuous lines are the fitting of the ANN.

To visualize the complexity of the problem being analyzed and tackled with the ANN, Fig. 5 shows a three-dimensions

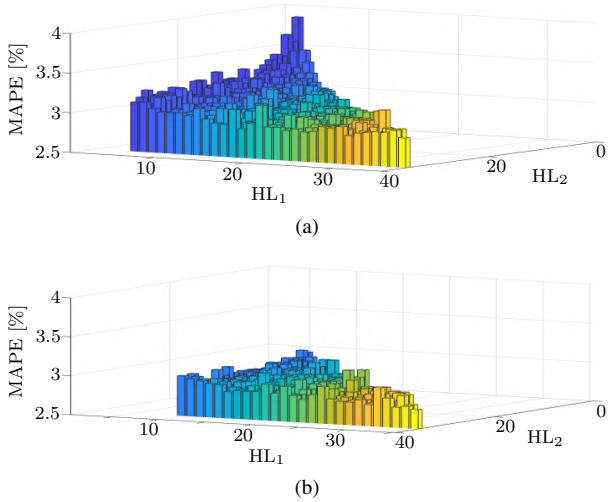

Fig. 3: Errors as a function of number of neurons in HL_1 and HL_2, in (a) with two hidden layers and in (b) with 10 neurons on the third hidden layer.

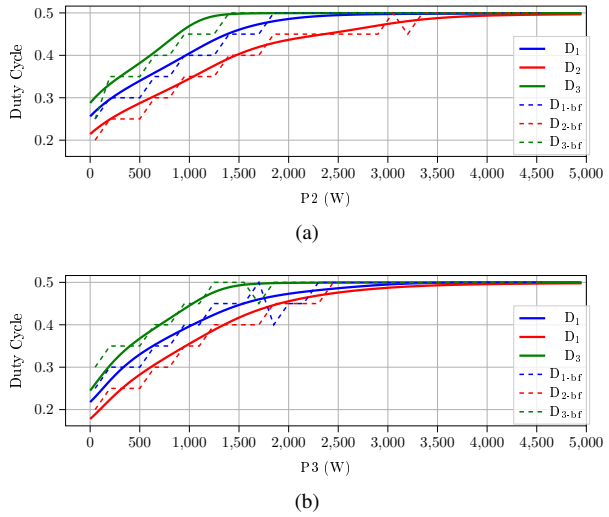

Fig. 4: Fitting of the ANN compared to brute-force analysis, in (a) with V_2=400 V, V_3=320 V and P_3=500 W and in (b) with V_2=400 V, V_3=320 V and P_2=500 W.

surface of the three duty-cycles when voltage V_2 and V_3 are kept constant.

VI. Experimental Results

A. Laboratory Prototype

To verify the proposed ANN approach, the experimental setup in Fig. 6 with a TAB converter prototype with parameters listed in Tab. III and structure in Fig. 7 was built.

Port-1 of the converter is connected to a fixed dc power supply at the rated voltage V_1 =400 V, while port-2 and port-3 are connected to corresponding dc electronic loads. The ANN model and the converter control and modulation are implemented on an Imperix L.t.d. BoomBox controller driving six Imperix PEB8032-A half-bridges.

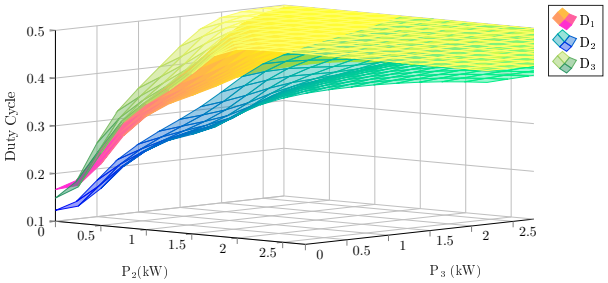

Fig. 5: Duty-cycles as a function of power with V_2=320 V and V_3=400 V.

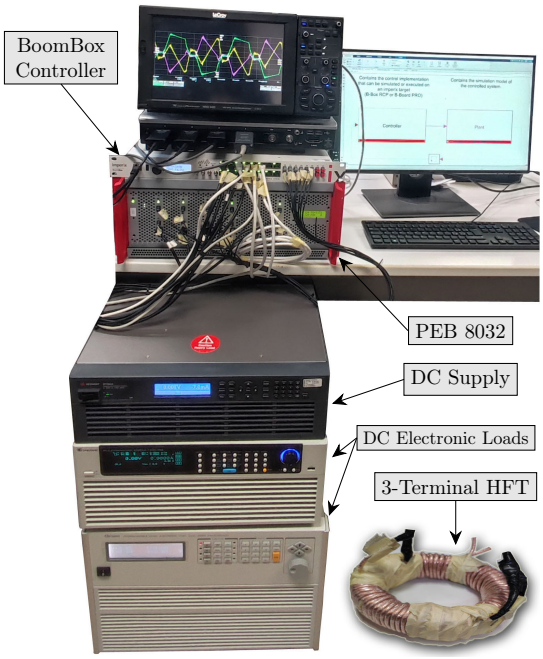

Fig. 6: Laboratory prototype of TAB.

In order to find the five modulation parameters for each set-point, two phase-shifts ϕ_2 and ϕ_3 are adjusted by employing two separate linear regulators followed by a decoupling matrix, as in [12]. While the duty-cycles D_1, D_2, and D_3 are generated from the ANN. The generated duty-cycles correspond to the optimum duty-cycles for the specific operating condition considered. The ANN model is run at a rate of 10 kHz, that is, 25 % of the switching and control frequency.

B. Results and Discussion

Sixteen cases are tested with a wide range of transferred power and a wide mismatch between the ports dc voltages, showing the merits of the proposed ANN-based modulation over the PSM. The test cases present the following voltage levels V_1 =400 V, V_2 =320 V, and V_3 =480 V, with port-2 power fixed at P_2 =350 W, and changing port-3 power in range from P_3 =200 W, to P_3 =3650 W.

Fig. 8 shows the optimum duty-cycles found experimentally for the sixteen test cases by the proposed ANN model as compared to those found by the brute-force search using simulation.

TABLE III: Experimental Prototype Parameters

Parameters		**Value**
Nominal power at each port P_{rated}	kW	5
Switching frequency $f_S = 1/T_S$	kHz	40
Rated dc voltages $V_1 = V_2 = V_3$	V	400
Transf. turns ratio $n_1 : n_2 : n_3$		1:1:1
Transf. leakage inductances:		
Port-1 leakage inductance L_1	µH	40
Port-1 leakage inductance L_2	µH	47
Port-1 leakage inductance L_3	µH	41
Dead time	µs	1
Switching Devices		MMIX1Y100N120C3H1

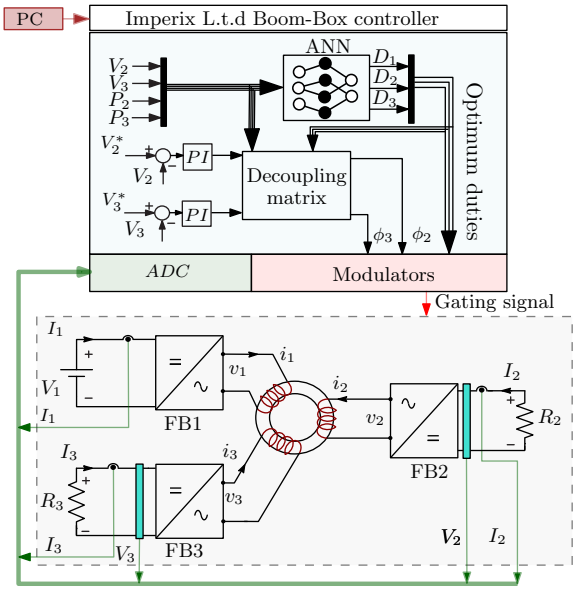

Fig. 7: Structure of the experimental setup.

Fig. 9 illustrates a comparison between the PSM and the proposed ANN-based modulation in terms of total true rms current. The proposed ANN-based modulation reduces the total true rms current by over 50% of its value at light load conditions.

Finally, Fig. 10 and Fig. 11 show the voltage and current waveforms of the PSM and the proposed ANN-based modulation for two test cases out of the sixteen at port-3 power P_3 =200 W and P_3 =1400 W, respectively. As shown in Fig. 10, the total true rms current reduces from about 8.3 A using PSM to about 3.9 A using the proposed ANN-based modulation, reducing the total true rms current by about 53% of its value. While the total rms current reduction of Fig. 11 is about 19%; as for the high power levels, the optimum operating point is located nearby the full duty modulation.

VII. Conclusion

An artificial neural network (ANN) approach for achieving reduced rms operation of triple active bridges (TAB) converters has been proposed and verified in this paper. A

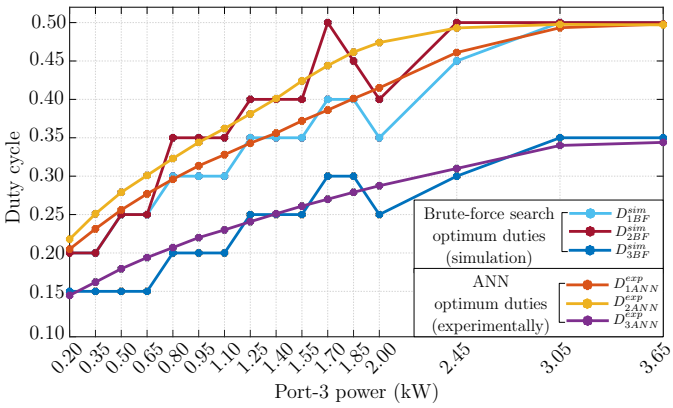

Fig. 8: Optimum duty-cycles found experimentally by the proposed ANN model versus those found by simulation brute-force search.

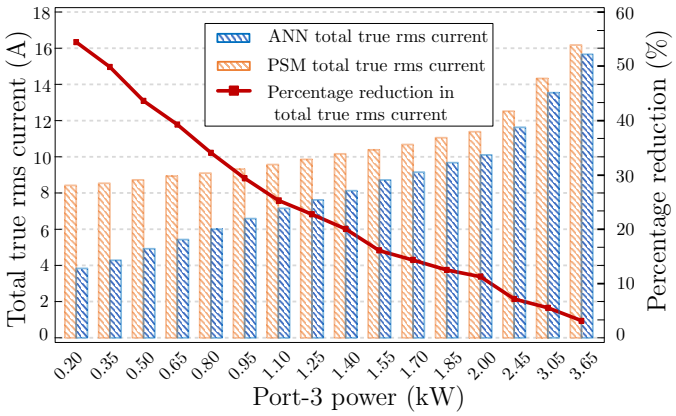

Fig. 9: Comparison in terms of total true rms current, as defined in (1), between PSM and the proposed ANN-based modulation, at $V_1 = 400\,\text{V}$, $V_2 = 320\,\text{V}$, $V_3 = 480\,\text{V}$, $P_2 = 350\,\text{W}$, and variable P_3.

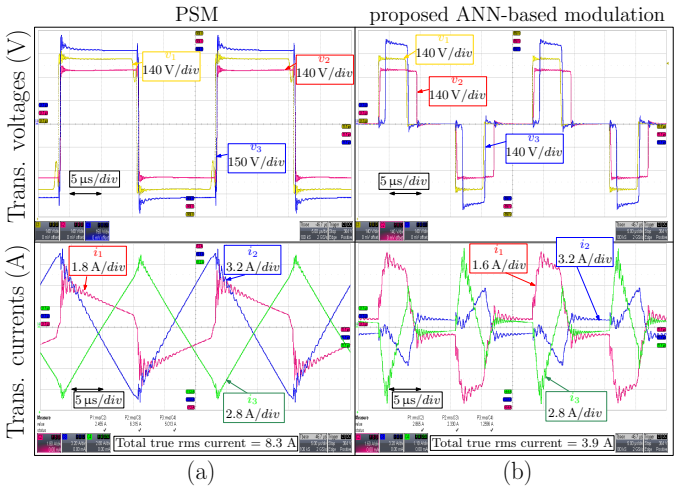

Fig. 10: Voltage and current waveforms with $V_1 = 400\,\text{V}$, $V_2 = 320\,\text{V}$, $V_3 = 480\,\text{V}$, $P_2 = 350\,\text{W}$, and $P_3 = 200\,\text{W}$: (a) using PSM; (b) using the proposed ANN-based modulation.

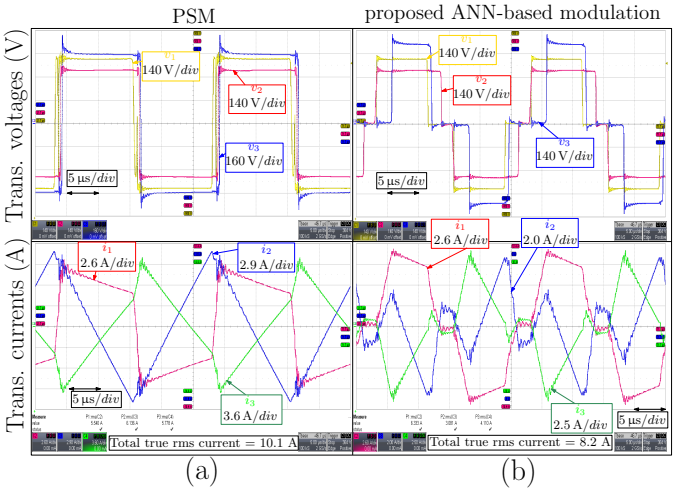

Fig. 11: Voltage and current waveforms with $V_1 = 400\,\mathrm{V}$, $V_2 = 320\,\mathrm{V}$, $V_3 = 480\,\mathrm{V}$, $P_2 = 350\,\mathrm{W}$, and $P_3 = 1400\,\mathrm{W}$: (a) using PSM; (b) using the proposed ANN-based modulation.

multilayer perceptron neural network was designed and trained in order to estimate the optimal modulation parameters of the TAB, aiming at converter operation with minimum total true rms currents. The ANN was trained based on a data-set generated by means of a simulation model. The simulation model was preliminarily calibrated to represent the real TAB implementation operation accurately. The approach features ease of data generation for ANN training, and deployability in real converter hardware, and allows significant improvements in terms of total rms current circulation compared to the classical phase shift approach. The proposed ANN approach shows other potential benefits with respect to the use of a look-up table for the modulation of the converter, including, smooth operation under different operating points, lower memory requirements, extension to converters with multiple ports, and the possibility of tuning the model with a reasonably limited number of samples of operating points.

VIII. Acknowledgments

This work was supported in part by the project Multiport-Grid "Cross-Sectoral Energy Control through Interconnected Microgrids by Multiport Converter" funded within the call "ERA-Net Smart Energy Systems RegSys Joint Call 2018" and in part by the project "Interdisciplinary Strategy for the Development of Advanced Mechatronics Technologies (SISTEMA)", DTG, University of Padova - Project code CUP-C36C18000400001.

References

[1] M. Rashidi *et al.*, "Design and Development of a High-Frequency Multiport Solid-State Transformer With Decoupled Control Scheme," *IEEE Trans. Ind. Appl.*, vol. 55, no. 6, pp. 7515–7526, 2019.

[2] T. Pereira *et al.*, "A Comprehensive Assessment of Multiwinding Transformer-Based DC–DC Converters," *IEEE Trans. Power Electron.*, vol. 36, no. 9, pp. 10 020–10 036, 2021.

[3] A. Avila *et al.*, "A Modular Multifunction Power Converter Based on a Multiwinding Flyback Transformer for EV Application," *IEEE Trans. Transport. Electrific.*, vol. 8, no. 1, pp. 168–179, 2022.

[4] C. Gu *et al.*, "A Multiport Power Conversion System for the More Electric Aircraft," *IEEE Trans. Transport. Electrific.*, vol. 6, no. 4, pp. 1707–1720, 2020.

[5] N. Swaminathan and Y. Cao, "An Overview of High-Conversion High-Voltage DC–DC Converters for Electrified Aviation Power Distribution System," *IEEE Trans. Transport. Electrific.*, vol. 6, no. 4, pp. 1740–1754, 2020.

[6] C. Samende *et al.*, "Power Loss Minimization of Off-Grid Solar DC Nano-Grids—Part I: Centralized Control Algorithm," *IEEE Trans. Smart Grid*, vol. 12, no. 6, pp. 4715–4725, 2021.

[7] A. Vettuparambil *et al.*, "A Modular Multiport Converter to Integrate Multiple Solar Photo-Voltaic (PV) Modules With a Battery Storage System and a DC Microgrid," *IEEE Trans. Ind. Electron.*, vol. 69, no. 5, pp. 4869–4878, 2022.

[8] J. Zeng *et al.*, "A Multiport Bidirectional DC–DC Converter for Hybrid Renewable Energy System Integration," *IEEE Trans. Power Electron.*, vol. 36, no. 11, pp. 12 281–12 291, 2021.

[9] Chuanhong Zhao and J. W. Kolar, "A Novel Three-Phase Three-Port UPS Employing a Single High-Frequency Isolation Transformer," in *2004 IEEE 35th Ann. Power Electron. Specialists Conf.*, vol. 6, 2004, pp. 4135–4141 Vol.6.

[10] M. Michon *et al.*, "A three-port bi-directional converter for hybrid fuel cell systems," in *2004 IEEE 35th Ann. Power Electron. Specialists Conf.*, vol. 6, 2004, pp. 4736–4742 Vol.6.

[11] F. Krismer and J. W. Kolar, "Closed Form Solution for Minimum Conduction Loss Modulation of DAB Converters," *IEEE Trans. Power Electron.*, vol. 27, no. 1, pp. 174–188, 2012.

[12] C. Zhao *et al.*, "An Isolated Three-Port Bidirectional DC-DC Converter With Decoupled Power Flow Management," *IEEE Trans. Power Electron.*, vol. 23, no. 5, pp. 2443–2453, 2008.

[13] A. A. Ibrahim *et al.*, "Conduction Loss Reduction of Isolated Bidirectional DC-DC Triple Active Bridge," in *2021 IEEE 4-th Intern. Conf. on DC Microgrids (ICDCM)*, 2021, pp. 1–8.

[14] P. Purgat *et al.*, "Zero Voltage Switching Criteria of Triple Active Bridge Converter," *IEEE Trans. Power Electron.*, vol. 36, no. 5, pp. 5425–5439, 2021.

[15] J. Li *et al.*, "Efficiency Optimization Scheme for Isolated Triple Active Bridge DC-DC Converter with Full Soft-Switching and Minimized RMS Current." *IEEE Trans. Power Electron.*, pp. 1–1, 2022.

[16] S. Dey and A. Mallik, "Multivariable-Modulation-Based Conduction Loss Minimization in a Triple-Active-Bridge Converter," *IEEE Trans. Power Electron.*, vol. 37, no. 6, pp. 6599–6612, 2022.

[17] S. Dey *et al.*, "Multi-variable Multi-constraint Optimization of Triple Active Bridge DC-DC Converter with Conduction Loss Minimization," *2022 IEEE Appl. Power Electron. Conf. & Expo (APEC)*, 2022.

[18] A. Chandwani and A. Mallik, "Three-loop Multi-variable Control of Triple Active Bridge Converter with Power Flow Optimization," *2022 IEEE Appl. Power Electron. Conf. & Expo (APEC)*, 2022.

[19] I. Kougioulis *et al.*, "An Integrated On-Board Charger and Auxiliary-Power Module for Electric Vehicles," *2022 IEEE Appl. Power Electron. Conf. & Expo (APEC)*, 2022.

[20] F. Toniolo *et al.*, "Implementation and experimental evaluation of an efficiency-improved modulation technique for IBCI DC-DC converters," in *2020 IEEE Appl. Power Electron. Conf. & Expo. (APEC)*. IEEE, 2020, pp. 3430–3436.

[21] X. Li *et al.*, "Artificial-Intelligence-Based Triple Phase Shift Modulation for Dual Active Bridge Converter with Minimized Current Stress," *IEEE Trans. Emerg. Sel. Topics Power Electron.*, 2021.

[22] S. Zhao *et al.*, "An Overview of Artificial Intelligence Applications for Power Electronics," *IEEE Trans. Power Electron.*, vol. 36, no. 4, pp. 4633–4658, 2021.

[23] F. Murtagh, "Multilayer perceptrons for classification and regression," *Neurocomputing*, vol. 2, pp. 183–197, 1991.

[24] P. G. Benardos and G.-C. Vosniakos, "Optimizing feedforward artificial neural network architecture," *Engineering applications of artificial intelligence*, vol. 20, pp. 365–382, 2007.

[25] S. Sharma *et al.*, "Activation Functions in Neural Networks," *Inter. Jour. of Eng. Appl. Sciences & Tech.*, vol. 4, pp. 310–316, 2020. [Online]. Available: http://www.ijeast.com